Depth Profiling of Residual Stress Distribution in Surface Treated Metallic Structures Using Nonlinear Ultrasonics

Santhakumar Sampath, Hongfei Liu, Zi Wen Tham, Yi Fan Chen and Lei Zhang*

Institute of Materials Research and Engineering (IMRE), Agency for Science, Technology and Research (A*STAR), 2 Fusionopolis Way, Innovis #08-03, Singapore 138634, Republic of Singapore

* Corresponding author

zhangl@imre.a-star.edu.sg

Abstract

Robotic hammer peening (RHP) is a cold-working technique to improve the fatigue life of metallic structures by inducing compressive residual stress in the near-surface region. Measuring the depth profiling of residual stress distribution plays an important role in process design towards the advanced manufacturing of metallic components. This study investigates the use of the nonlinear ultrasonic method to measure the residual stress profiles through the frequency-dependent penetration depth approach. Stainless steel specimens were treated with varying RHP intensities, and their morphological evolutions were characterized with a step-profilometer. The amplitudes of the second and third harmonic components of the longitudinal critically refracted (LCR) and Rayleigh waves were measured and analyzed. The effect of the surface roughness on the nonlinearity parameters before and after polishing at various peening intensities was briefly discussed. The results show a large variation in the acoustic nonlinearity parameter at the surface layer, indicating the potential of the proposed nonlinear ultrasonics for the measurement of depth profiling of residual stress.

Keywords: Longitudinal critically refracted (LCR) waves; Rayleigh waves; Robotic hammer peening; Residual stress profile; Nonlinear ultrasonics; Surface roughness

1. Introduction

In metallic structures, most failures, such as fatigue cracks, typically begin on the surface or near-surface regions [1-3]. To improve the fatigue life of a structure, a cold-working technique is often employed, during which external mechanical forces are applied to the surfaces of structures [4-6]. The main purpose of this process is to introduce compressive residual stress in the near-surface region, which can inhibit pitting initiation and propagation [7, 8]. Consequently, the fatigue crack initiation can be effectively prevented. Nonetheless, to maintain the stress balance, the generation of compressive residual stresses can lead to the development of tensile residual stresses in deeper regions of the structure [9]. This can have a detrimental effect on mechanical performance. Therefore, it is essential to measure the residual stress profiles of structures to evaluate their service reliability. The non-destructive measurement of near-surface residual stresses can provide valuable insights into the fatigue life of surface-enhanced structures.

Cold-working techniques, including shot peening [10], robotic hammer peening (RHP) [11], deep cold rolling [12], and laser-shock peening [13] are commonly used to improve the surface characteristics of metallic structures. More specifically, RHP is a fast-growing surface treatment process that involves impacting the specimen surface with a high oscillation frequency shot, resulting in plastic deformation and inducing substantial residual stress [14]. Compared with other peening techniques, RHP can generate a deeper residual stress and a more uniform stress distribution [15], making it a cost-effective method for increasing the fatigue life of metallic structures. Furthermore, the repeated impacts associated with the RHP generate residual stress fields near the surface, which allows plastic deformation to take place on the surface adjacent to an elastic zone and prevents dilatation of the deformed region. The combination of RHP with

robot-based direct energy deposition, such as laser-cladding [16], has attracted research interest in this process as well as the rapid growth of additive manufacturing in recent years [17, 18].

To date, various non-destructive methods have been developed to measure residual stress, such as X-ray diffraction (XRD), neutron diffraction, and ultrasonic methods [19, 20]. Among them, XRD is widely employed for determining the depth profile of residual stress according to Bragg's law [6, 21]. However, its application is restricted to near-surface stress measurements because of the limited penetration depth of X-ray beams [22], meaning that layer removal by electropolishing is required to acquire the residual-stress profile, which is a lengthy process [6]. Furthermore, localized variations in the residual stress field may still be missed if their wavelengths are significantly smaller than the diffraction area. The principle of residual stress measurement employing neutron diffraction is analogous to that of XRD. However, XRD is only capable of measuring average stress over a few microns close to the surface, whereas neutron diffraction can measure residual stress across material layers [23, 24]. Daymond and Bonner [25] investigated the residual stress in a titanium linear friction weld using pulsed neutron diffraction as a function of distance from the weld zone. Mohammad Masoomi et al. [26] studied the effect of heat treatment on the residual stress distribution in stainless steel 17-4 PH manufactured using the laser powder bed fusion method. Brown et al. [27, 28] utilized a SMARTS diffractometer that emits a white neutron beam to examine the remaining tension in Al Cladding containing U-10Mo fuel foil components. Their discoveries revealed that cladding decreases the dislocation density of the material. Despite its benefits, the neutron diffraction technique has some disadvantages such as long measurement time, and high cost of neutron source development.

Ultrasonic method for residual stress estimation in surface-enhanced structures has a noteworthy potential [29]. This method is based on the acoustoelastic effect, which relies on the

use of ultrasonic surface waves, such as longitudinal critically refracted (LCR) and Rayleigh waves, to determine the wave velocity changes relative to the stress [30, 31]. These waves travel along the surface, penetrating the structure to a depth of approximately one wavelength (λ) [32], allowing for the evaluation of the residual stress profile near the surface. Although LCR waves have been extensively studied, the effect of residual stress on the variation in LCR velocity is minimal [33], leading to a large error in the resulting stress measurements [34]. Rayleigh wave acoustoelastic effect has been investigated both theoretically [30] and experimentally [35] and experimentally [36]. For example, Hirao et al. [37] discussed a case in which the initial stress varied with the depth below the surface of the structure. However, estimating the residual-stress using third-order elastic constants remains difficult [38]. Zhan et al. [39] employed a laser ultrasonic technique to evaluate the residual stress in TC4 alloy materials, and their results indicated a noticeable impact of the cooling rate and solution temperature on the magnitude of the residual stress. Liu et al. [40] utilized Rayleigh dispersion approach to examine the inverse of residual stress in ground silicon wafers. Nevertheless, owing to multi-modal characteristics [41], and dispersion properties [42], research on the use of ultrasonic guided waves for the assessment of material residual stress has been restricted.

Compared with the linear ultrasonic method, the nonlinear ultrasonic method is more sensitive to microstructural changes in the material [43, 44]. When surface waves interact with a peened structure containing residual stress-induced nonlinearity, harmonic components are generated, including second and third harmonics [45, 46]. Consequently, the acoustic nonlinearity parameter can be used to measure the residual stress because it is proportional to the amplitude of harmonic components [47]. This parameter has proven to be effective in assessing the damage related to plastic deformation [48] and creep degradation [49]. The estimation of not only the surface residual

stress but also the profile of penetration of the stress layer, particularly the maximum compressive residual stress and its locations, is an important requirement for predicting the lifetimes of materials. To date, most studies have been carried out on the nonlinear ultrasonics of LCR waves to establish a correlation between the average residual stress and nonlinear parameters such as the second harmonics [50, 51].

This study aimed to evaluate the depth profile of residual stress in peened specimens using nonlinear ultrasonics of LCR and Rayleigh waves. The frequency-dependent penetration depth approach was used to extract the residual stress profile by adjusting the excitation frequencies from 1 MHz to 5 MHz. A theoretical model was used to investigate the propagation of surface waves (LCR and Rayleigh waves) in peened specimens, and the relationship between the acoustic nonlinearity parameter and the residual stress was presented. Additionally, experiments using nonlinear surface waves were conducted on stainless steel specimens with different peening intensities. Finally, the influence of the surface roughness of the specimens on the nonlinear parameters before and after polishing at various peening intensities was discussed.

2. Theory

2.1 Depth profiling of residual stress

The propagation of nonlinear surface waves, such as LCR and Rayleigh waves, was proposed in this study to evaluate the residual stress at different depths in surface-treated materials. RHP is a process that modifies the near-surface region with plastic deformation to induce compressive residual stresses to enhance fatigue life. When an input surface wave traveling at a certain frequency is applied to an ideal linear material, the response of the material is only a linear component, corresponding to the input frequency. However, if the material exhibits nonlinear behavior owing to the presence of residual stress, the response contains harmonic components,

such as second, third, and higher harmonics, in addition to the linear component. The propagation depth of surface waves can be related to the excitation frequency, and typically penetrates one wavelength (λ) into the material [52]. It is possible to obtain the residual stress at different depths below the material surface by altering the excitation frequency, as illustrated in Fig. 1. However, there is no accurate formula for determining propagation depth. The empirical formula based on the experimental results is derived as follows [53]:

$$d = \frac{v}{f^{0.96}} \tag{1}$$

where v is ultrasonic wave velocity, d denotes the penetration depth, and f is the input frequency. In Fig. 1(b), it is observed that when the excitation frequency is $f_1 > f_2$, the propagation depth of the surface wave is $d_1 < d_2$ [54]. This implies that when the surface wave is excited at f_1, the surface wave covers a layer depth of approximately d_1. The measured residual stress was averaged within the depth of d_1. To obtain the residual stress distribution in depth, this study proposes the difference in propagation depths between the two excitation frequencies, which is expressed as:

$$\Delta d_k = d_j - d_i = v\left(\frac{1}{f_j^{0.96}} - \frac{1}{f_i^{0.96}}\right);\ f_i > f_j \tag{2}$$

where Δd_k provides the residual stress information within the propagation depth of $d_j - d_i$, where i, j and k are equal to 1, 2, 3 and so on. For example, Δd_1 can be estimated from $d_2 - d_1$ when the excitation frequencies are f_2 and f_1. Similarly, Δd_2 and Δd_3 were estimated from excitation frequencies of f_2, f_3 and f_4 ($f_2 > f_3 > f_4$).

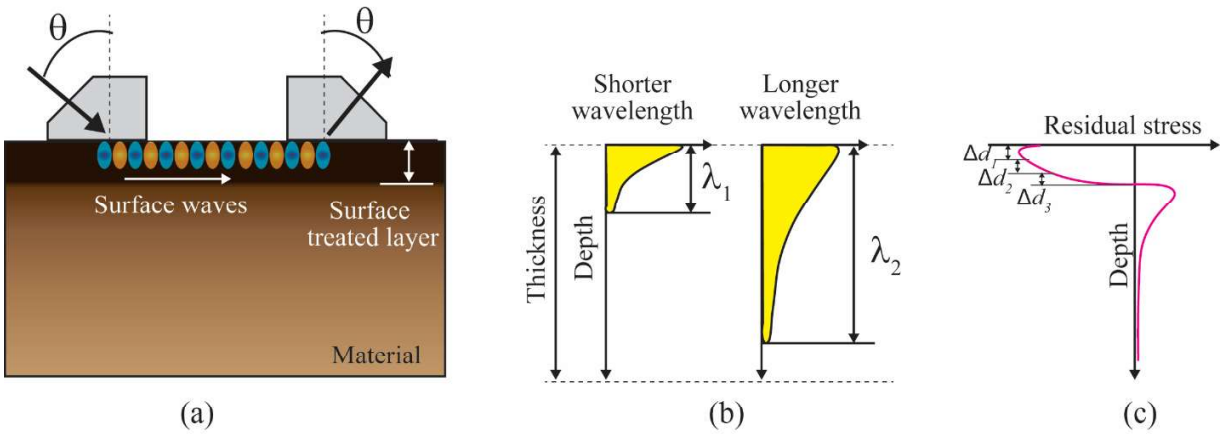

Fig. 1. (a) Surface wave generation and the corresponding detection method, (b) penetration depths of the surface waves in surface-treated specimens with respect to the wavelength and (c) proposed residual stress extraction approach from difference of two excitation frequencies.

According to Snell's law, the relationship between the incident angle and ultrasonic wave velocity can be expressed as

$$\theta = \sin^{-1}\left(\frac{v_1}{v_2}\right) \tag{3}$$

where v_1 and v_2 are ultrasonic wave velocities in the wedge and the specimen, respectively, and θ denotes the incident angle. In this study, the longitudinal wave velocity of the wedge was determined as approximately 2730 m/s, whereas that of the steel specimen was measured as approximately 5662 m/s. According to Eq. (3), an LCR wave can be formed in the specimen when the incident angle approaches the first critical angle, whereas Rayleigh waves are produced when the incident angle is equal to or greater than the second critical angle [55].

2.2 Characterization acoustic nonlinearity parameters of surface treated layer

The equations governing the motion of a solid in the absence of external forces can be written as follows [56]:

$$\rho_0 \frac{\partial^2 u_i}{\partial t^2} = \frac{\partial \sigma_{ij}}{\partial x} \tag{4}$$

where ρ_0 is the initial density, u_i is the particle displacement, t is the time, σ_{ij} is the first Piola-Kirchhoff stress and x is the coordinate of the particle deformation. The first Piola-Kirchhoff stress is expressed as follows:

$$\sigma_{ij} = \sigma_{ij}^0 + A_{ijkl}\frac{\partial u}{\partial x} + \frac{1}{2}A_{ijklmn}\frac{\partial^2 u}{\partial x^2} \tag{5}$$

where σ_{ij}^0 denotes the residual stress of the peened material. A_{ijkl} and A_{ijklmn} are second- and third-order Huang coefficients, respectively [57] and are expressed by $A_{ijkl} = \sigma_{ji}^0\delta_{ik} + C_{ijkl}$ and $A_{ijklmn} = C_{ijklmn} + C_{ijln}\delta_{km} + C_{jnkl}\delta_{im} + C_{jlmn}\delta_{ik}$. The expressions for A_{ijkl} and A_{ijklmn} are presented in terms of residual stress in [58]. Here, C_{ijkl} and C_{ijklmn} are the Brugger second-, third-, and fourth-order moduli tensors defining the third- and fourth-order elastic constants, respectively. Moreover, the one-dimensional ultrasonic wave propagation in an isotropic solid was obtained by substituting Eq. (5) into Eq. (4):

$$\frac{\partial^2 u}{\partial t^2} = M_2\frac{\partial^2 u}{\partial x^2} + M_3\left(\frac{\partial u}{\partial x}\right)\frac{\partial^2 u}{\partial x^2} + M_4\left(\frac{\partial u}{\partial x}\right)^2\frac{\partial^2 u}{\partial x^2} + \cdots \tag{6}$$

where

$$\begin{aligned} M_2 &= C_{11} \\ M_3 &= 3C_{11} + C_{111} \\ M_4 &= \frac{3}{2}C_{11} + 3C_{111} + \frac{1}{2}C_{1111} \end{aligned} \tag{7}$$

The relationship between the Brugger constants and elastic constants can be established as follows [45]: $c_{11} = \lambda + 2\mu$, $c_{111} = 2l + 4m$, $c_{1111} = 24p$. Here, λ and μ are the Lamé elastic constants, and l, m and p are the third- and fourth-order elastic constants, respectively. Eq. (7) can be rewritten in a form that includes second-order (β) and third-order (γ) nonlinearity parameters as follows [59, 60]:

$$\frac{\partial^2 u}{\partial t^2} = C_{11}\frac{\partial^2 u}{\partial x^2} + \beta C_{11}\left(\frac{\partial u}{\partial x}\right)\frac{\partial^2 u}{\partial x^2} + \gamma C_{11}\left(\frac{\partial u}{\partial x}\right)^2\frac{\partial^2 u}{\partial x^2} + \cdots \tag{8}$$

where

$$\beta = -\left(\frac{C_{111}}{C_{11} + \sigma_{11}^R}\right)$$
$$\gamma = -\frac{1}{2}\left(\frac{3C_{11} + 6C_{111} + C_{1111}}{C_{11} + \sigma_{11}^R}\right) \tag{9}$$

In Eq. (9), when the peening intensity is increased, the residual stress σ_{11}^R also increases, although it remains negligible in comparison to the elastic constants. The third-order elastic constant, C_{1111}, is highly dependent on the plastic deformation that occurs in the material, whereas the second-order elastic constant, C_{111}, has negligible dependence on plastic deformation. Generally, β increases with increasing plastic deformation, although the actual relationship is complex. The plasticity of the surface is caused by peening, which is associated with the compressive surface residual stress and can be determined from the calculated value of β; β and γ can be expressed using the perturbation solution as follows [61]:

$$\beta = \frac{8}{k^2 x}\frac{A_{2f}}{A_f^2}$$
$$\gamma = \frac{32}{k^4 x^2}\frac{A_{3f}}{A_f^3} \tag{10}$$

where x is the distance of the surface wave propagation, and A_f, A_{2f}, and A_{3f} are the amplitudes of the fundamental, second, and third harmonics, respectively. Because the propagating distance (x) and wavenumber (k) were kept constant during the experiments, Eq. (10) can be simplified as follows [62]

$$\beta' = \frac{A_{2f}}{A_f^2} \tag{11}$$

$$\gamma' = \frac{A_{3f}}{A_f^3}$$

For this study, surface waves were used to measure β' and γ', which allowed characterization of the surface residual stress profile. It should be noted that the parameter γ' depends on both the third- and fourth-order elastic moduli, but its dependence on the fourth-order elastic constants is weak. As a result, parameter γ' becomes equal to the square of parameter β' when the fourth-order elastic modulus is neglected [63].

3. Experimental procedures

3.1 Robotic hammer peening (RHP) process

Ten stainless steel specimens (SS304L) were subjected to different RHP processes and denoted as RHP-1, RHP-2, RHP-3, RHP-4, and RHP-5. The dimensions of the specimens were 200 mm × 50 mm × 10 mm, and their corresponding photographic images are shown in Fig. 2(a). The industrial robotic platform model IRB 6660 was used to perform the peening process as shown in Fig. 2(b). A spherical tungsten carbide hammer head, with a diameter of 5 mm and driving pressure of 4 bar, was employed. The impact frequency of the hammer head was set at approximately 200 Hz, with a stroke and standoff of 4 mm and 2 mm, respectively. The longitudinal feeding rate was fixed at 1000 mm/min, while the peening coverage was varied via the stepover distance with 400%, 1200%, 1600%, and 2000% for RHP-1, RHP-2, RHP-3, and RHP-4, respectively.

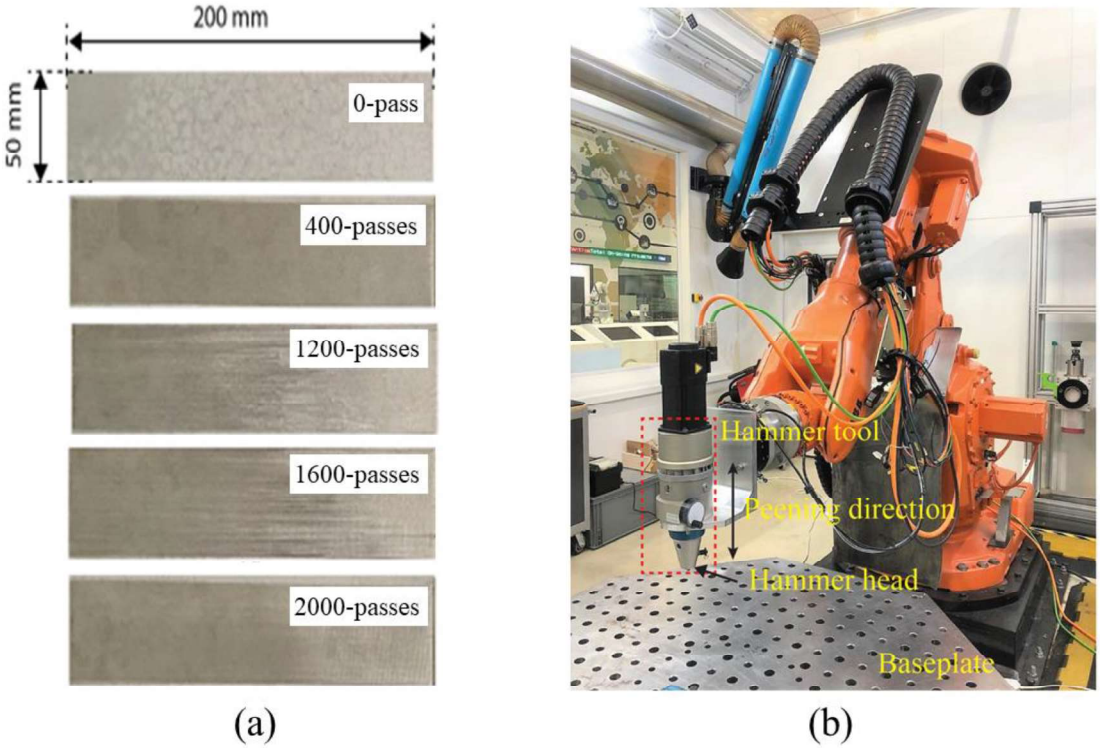

Fig. 2. (a) Dimensions and photographic images of the specimens: intact specimen (0-pass), RHP-1 (400-passes), RHP-2 (1200- passes), RHP-3 (1600- passes), and RHP-4 (2000- passes) and (a) photographic image of the robotic hammer peening system.

3.2 Nonlinear ultrasonic experiment

The experimental system for residual stress measurements employing nonlinear ultrasonic waves is depicted in Fig. 3. This system consists of a function generator (AFG31021, Tektronix, USA), an amplifier (CIPRIAN Model US-TXP-3), a pair of ultrasonic transmitter and receiver, and an oscilloscope (MSO5204, Tektronix, USA). The function generator was set to produce a tone burst signal in the form of a sine wave modulated by a Gaussian window function with 12 cycles to reduce the bandwidth of the input frequency in the frequency domain and avoid the overlap of the generated second- and third-harmonic components with the input frequency component. The peak-to-peak voltage of the signal was set at 50 mV. An amplifier was used to amplify the signal by a factor of 100 before it was sent to the transmitter. The oscilloscope with a sampling frequency of 2.5 GS/s digitized the signal received from the receiver before it was fed

into a computer. In addition, the signal received by the receiver is amplified using an amplifier. Moreover, 512 ultrasonic responses were recorded and averaged to improve the signal-to-noise ratio (SNR). Nine different excitation frequencies (1, 1.25, 1.5, 2, 2.25, 2.5, 3, 4, and 5 MHz) were utilized to evaluate the residual-stress profile.

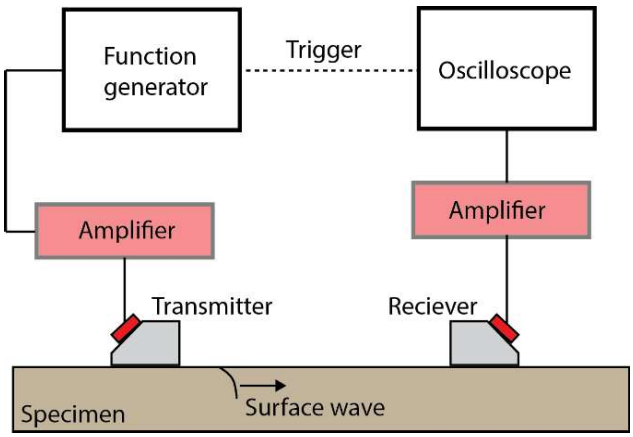

Fig. 3. The entire experimental setup: (a) Schematic view and (b) photographic view of the specimen and the transducer assembly.

Considering a frequency of 2.5 MHz and wave velocity of 5.6 km/s, the propagation depth of LCR was calculated to be 2.34 mm, which was consistent with the experimental result of penetration depth of LCR (Shunming et al. [55]). Additionally, the penetration depth of Rayleigh wave is roughly one wavelength [64]. When the excitation frequency was set to 2.0 MHz and the measured Rayleigh wave velocity was 2.7 km/s in stainless steel materials, the propagation depth was calculated to be 1.40 mm, thereby satisfying the requirements for detection.

3.3 Surface roughness measurement

The morphology of the specimens processed with RHP was observed under an optical microscope and their surface profiles and corresponding surface mappings were measured in contact mode using a step profilometer (KLA-Tencor). The surface roughness values of the specimens (pre- and post-polishing) were measured in the range of 1 mm × 1 mm square. Calibration of surface roughness was performed using an RHP-1 specimen with a surface

roughness of 4.87 μm. To evaluate the effects of the surface treatments on the morphology and surface roughness of the specimens, an optical microscope (BX51M, Olympus Co. Ltd.) was used for observation.

4. Results and discussion

4.1 Nonlinear ultrasonic measurements

Initially, the second and third harmonics of the surface waves generated by intact and peened specimens were investigated. Figure 4 shows the ultrasonic responses in the time- and frequency domains for the intact and peened (RHP-1) specimens when the receiver was located 180 mm from the transmitter. The propagation distance choice was based on the cumulative effect of attenuation of nonlinear components, which does not decrease within this range [45]. It was difficult to ascertain from the time domain signal if harmonic components were produced from residual stress-induced nonlinearity. However, analysis of the corresponding frequency spectra provided evidence of their presence. In the peened specimen, the second harmonic component ($2f$ = 10 MHz), and third harmonic component ($3f$ = 15 MHz) were visible. Conversely, the generation of harmonic components in an intact specimen is caused by intrinsic material nonlinearity (IMN) [65]. The presence of lattice anharmonicity, vacancies, or precipitates can lead to intrinsic material nonlinearity (IMN) in pristine materials [66]. From Fig. 4, it can also be seen that the amplitudes of the harmonic components due to IMN were significantly smaller than those of the harmonic components generated by the peened specimen. These findings suggest that the residual stress-induced nonlinearity is more prominent than that of the IMN in the peened specimen. For instance, the peak amplitude of the second harmonic component was higher for the peened specimen (0.13 mV) than for the intact specimen (0.08 mV) owing to the nonlinearity induced by the peening

process. Moreover, the relative amplitude variation of the third harmonic component was 24.5% larger than that of the second harmonic component.

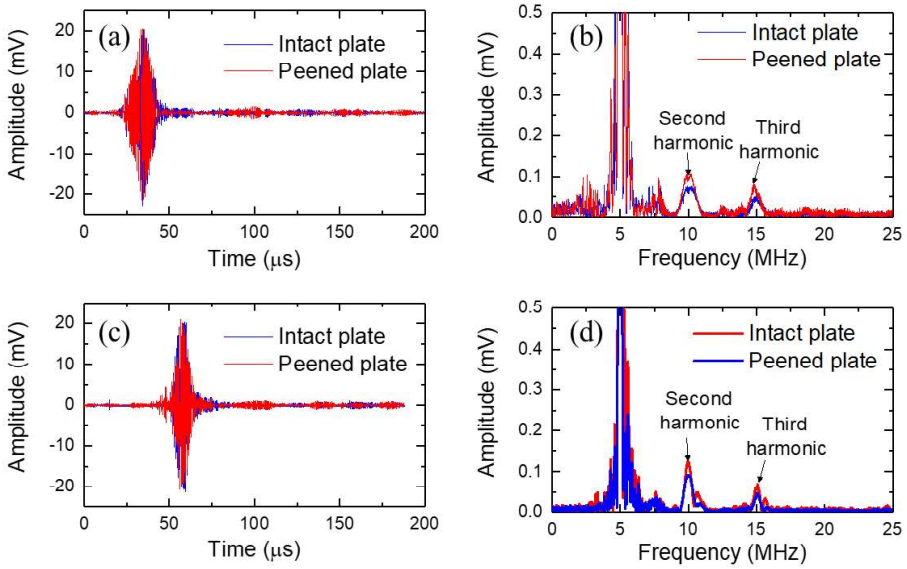

Fig. 4. Time domain and frequency domain responses for the intact specimen and the peened specimen (RHP-1) in which the receiver is located 180 mm from the transmitter: (a) time and (b) frequency domain of the LCR waves; (c) time and (d) frequency domain of the Rayleigh waves.

Figure 5 compare the nonlinear ultrasonic responses of the second and third harmonics of residual stress generated by LCR and Rayleigh waves. Ultrasonic responses were recorded when the LCR and Rayleigh waves were excited on the peened specimen (RHP-4) at three distinct frequencies (1, 2.5, and 5 MHz). The amplitudes of the input [$A_1(f)$], second [$A_2\ (2f)$] and third harmonic components [$A_3\ (3f)$] were employed to measure the acoustic nonlinearity parameters (β' and γ') [61]. It was observed that the amplitude of the input component was approximately 10 times higher than those of the second and third harmonic components. However, these harmonic components still had a signal-to-noise ratio of 10 dB, indicating they were well above the noise level. In addition, the variations in the amplitude of the linear components were found to be significantly smaller than those of the nonlinear components, as displayed in Figs. 4-5.

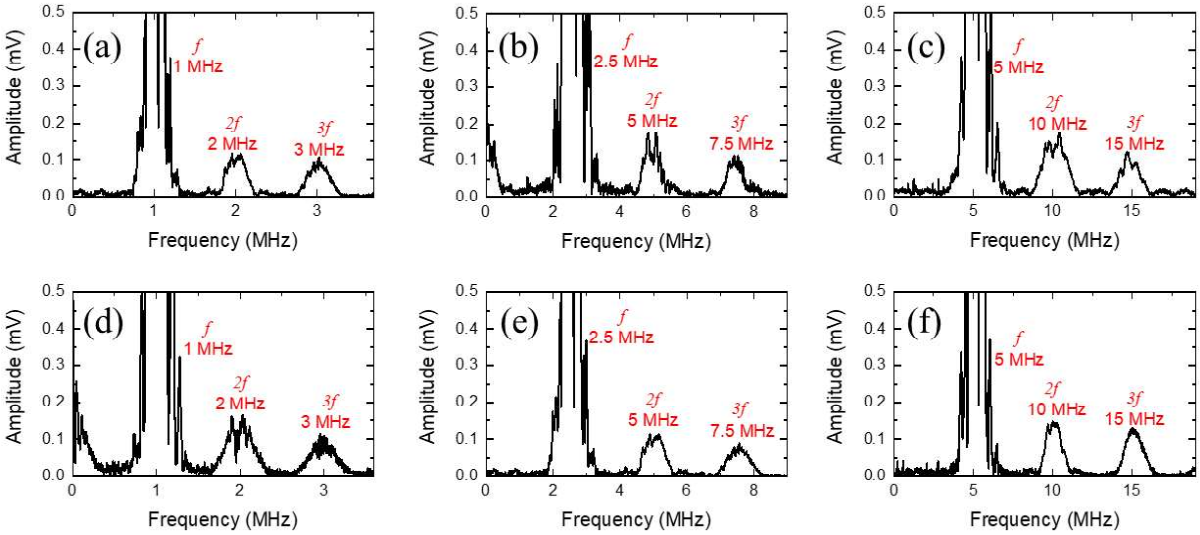

Fig. 5. A comparison of the frequency-domain obtained from the peened specimen (RHP-4) was conducted when the frequency of the excited LCR waves was set at (a) 1 MHz, (b) 2.5 MHz, and (c) 5 MHz, and the frequency of the excited Rayleigh waves was set at (d) 1 MHz, (e) 2.5 MHz, and (f) 5 MHz.

To further explore the effects of surface qualities on the sensitivities of the second and third harmonic components, the nonlinearity parameters β' and γ' were obtained (Fig. 6). For comparability, the parameters were normalized with respect to the values measured for the intact specimen. Error bars represent the standard deviation of the output responses obtained from the pair of four distinct peening process (from 400 to 2000-passess) specimens. These error bars highlight the variability in output responses. As evident from Figs. 6(a) and (c), the LCR waves exhibited greater sensitivity to residual stress than the Rayleigh waves in the case of the unpolished peened specimen. In contrast, the LCR waves were found to be less sensitive to the residual stress than the Rayleigh waves in the case of the polished peened specimens. Comparing the polished and unpolished specimens, an increase in γ' of the Rayleigh wave from 18.9 to 26.9% was observed for RHP-4. Additionally, it was determined that the variation in β' was extremely large for both surface waves in RHP-1 (Fig. 6(a)) and particularly small in the case of RHP-4. This can be attributed to the fact that the surface roughness of RHP-1 was greater than that of RHP-4.

Furthermore, the γ' parameter was more sensitive to the different peened specimens than β', as indicated by the larger percentage change in γ' than in β' (see Table 1).

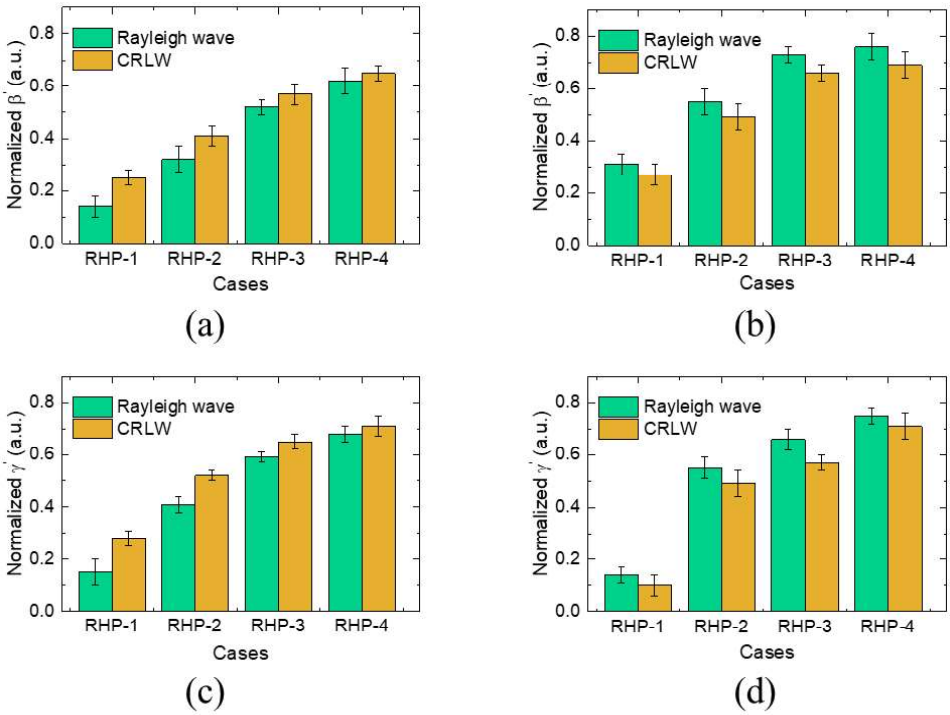

Fig. 6. Relationship between the normalized parameters and the different peening processes when the excitation frequency was set at 5 MHz. The β' parameter for (a) the unpolished peened specimens and (b) the polished peened specimens, the γ' parameter for (c) the unpolished peened specimens and (d) the polished peened specimens.

Table 1. Percentage changes of β' and γ' for the peened specimens subjected to different RHP processes.

RHP process	Percentage change of β'	Percentage change of γ'
RHP-1	12.8	17.5
RHP-2	22.6	25.3
RHP-3	26.4	32.2
RHP-4	31.7	36.4

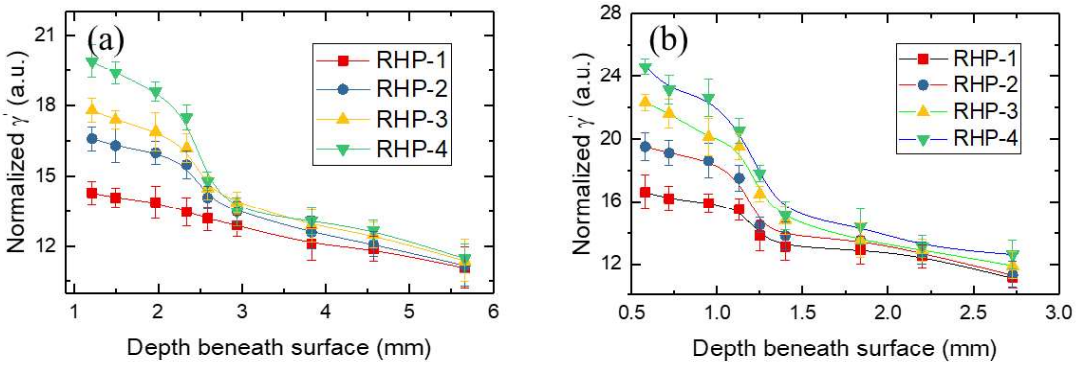

Fig. 7. Nonlinear ultrasonic measurement of the residual stress profiles with respect to depth. (a) LCR waves, and (b) Rayleigh waves.

Figure 7 is obtained by tuning the input excitation frequencies from 1 MHz to 5 MHz, resulting in a variation in the penetration depth of the corresponding input frequency from 2.73 mm to 0.58 mm. It was found that a lower penetration depth correlated with a higher γ', due to the presence of a maximum compressive residual stress. This revealed that the distribution of the residual stress in the depth direction could be acquired by gradually increasing frequency. As shown in Fig. 7, γ' as seen to decrease with increasing depth, which can provide insight into the residual stress. Comparatively, the RHP-4 specimen had a significantly higher γ' than the RHP-1 specimen, implying that the number of peening passes is a major factor in determining the degree of residual stress. Additionally, the maximum variation in γ' was observed at a depth of approximately 1 mm for LCR waves, and 0.5 mm for Rayleigh waves, which can be attributed to the maximum residual stress located near the surface. Notably, the magnitude of γ' on the surface increased from 15.3 to 20.9 as the number of peening passes increased from 400 to 2000 for LCR waves, and from 17.6 to 25.6 for Rayleigh waves. A comparison between the LCR and Rayleigh waves reveals notable differences in the value of γ'. This implies that the nonlinear Rayleigh wave can be effectively exploited to measure residual stress profiles. The RHP-4 specimen exhibits the highest residual stress at a level of about 580 μm below the surface, and the surface layer affected by RHP is around 200 μm [67]. Additionally, it was observed that increasing the peening intensity did not

significantly alter the surface layer thickness, but rather improved the maximum residual stress at the surface.

4.2 Discussion

To assess the impact of surface roughness on nonlinear ultrasonic parameters, a range of specimens were studied using a step-profilometer system. The results of this investigation, shown in Fig. 8, indicate that compared to the intact specimen, the surface roughness increased significantly following the RHP process. Furthermore, it was observed that the surface roughness varied in a two-stage process: (i) the surface roughness increased rapidly with the number of peening passes, likely due to the formation of craters and pileups; and (ii) the surface roughness decreased slightly as a result of the flattening effect of the higher energy applied for longer treatment times. Table 2 outlines the roughening effect of the peening process, demonstrating a 69.1% increase in the R_a values from 1.5 μm in the intact specimen to 4.87 μm for the RHP-1 specimen, and a 72.8% decrease in the R_a values from 1.5 μm in the intact specimen to 5.52 μm for the RHP-4 specimen. These results suggest that the RHP treatment is suitable for practical applications and is likely to improve the surface roughness of the material. Surface treated area of RHP-4 specimen after 1 min. is illustrated in Fig. 9, where the yellow dotted circles indicate the treated and untreated areas, respectively. As the peening time increases, the number of hammers impacting the surface also increases, resulting in the complete disappearance of the untreated area. Furthermore, plastic deformation was evident on the surface treated layer of the RHP-4 specimen, due to the reduced height between the peaks and valleys, which further improved the surface roughness.

Table 2. Surface roughness values of the different peened specimens.

RHP process	R_a (μm)	R_q (μm)	R_z (μm)

RHP-1	4.87	5.92	42.8
RHP-2	3.46	4.47	34.2
RHP-3	6.61	9.31	62.1
RHP-4	5.52	7.54	70.6

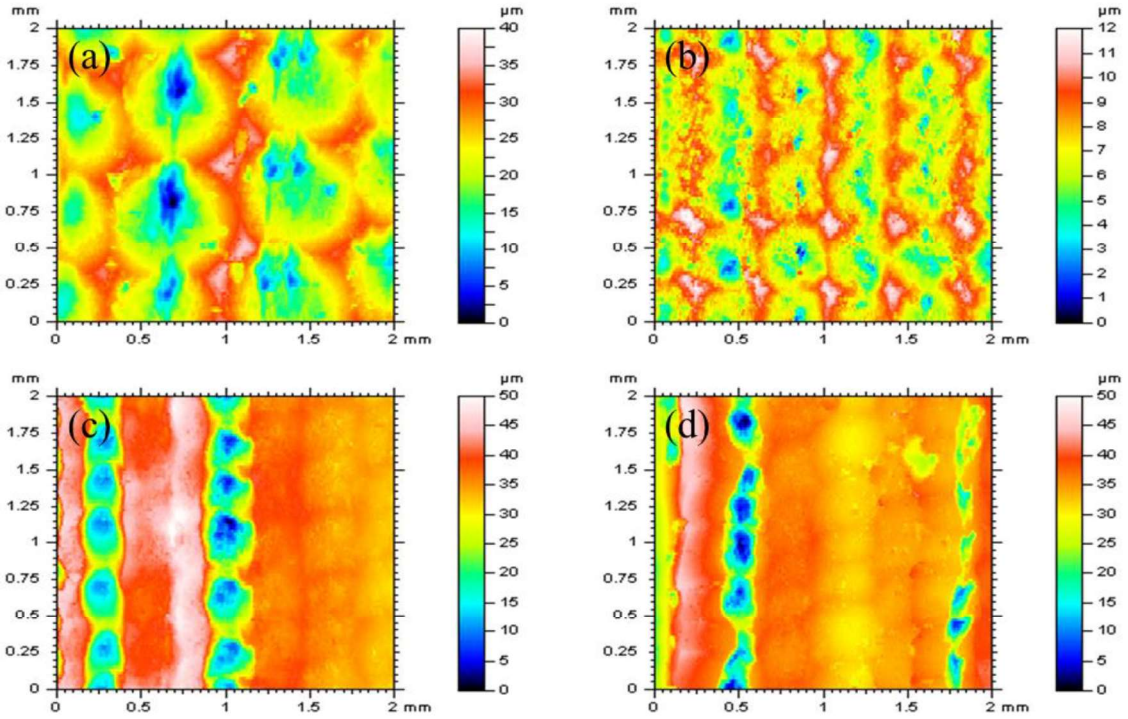

Fig. 8. Surface morphologies resulting from the different peening processes: (a) RHP-1, (b) RHP-2, (c) RHP- 3, and (d) RHP-4.

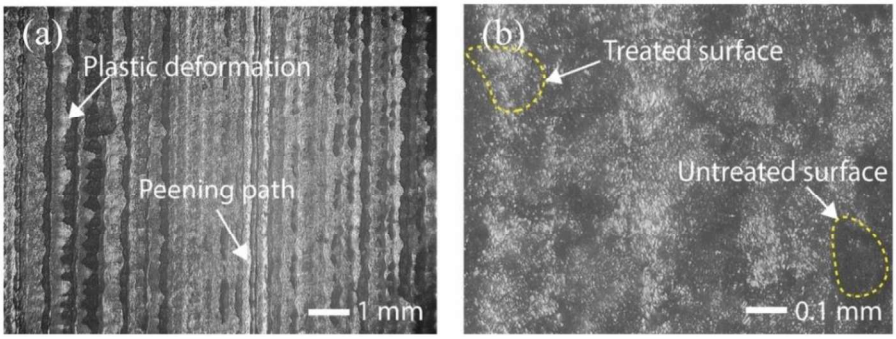

Fig. 9. Optical microscope images of the surface treated specimen (RHP-4) at different magnifications after RHP process. (a) 1 mm and (b) 0.1 mm.

The samples were hand-polished using fine polish papers with grit 600 and 1200. It is noted that the polishing process likely removes surface layers of approximately 10 μm, leading to a decrease in the surface roughness. Figure 10 shows the variation in the β' and γ' parameters before and after polishing the peened specimens. The slopes of β' obtained from the LCR waves before and after polishing were 25.6% and 28.9%, respectively, indicating that the nonlinearity parameters of the LCR waves are minimally affected by the surface quality of the specimen. In contrast, the gradients of the β' measured from the Rayleigh waves before and after polishing were 24.7% and 41.3%, respectively (Fig. 10(b)). This demonstrates that Rayleigh waves are more sensitive to the surface conditions of the specimen. As discussed above, the slope of the polished peened specimen was reduced from 81% to 44.5%, compared to the unpolished peened specimen. This suggests that polishing has a considerable effect on the residual stress profile, as evidenced by the change in the nonlinear parameters of Rayleigh wave, which are more sensitive to residual stress variations than those obtained from the LCR waves after polishing the specimen.

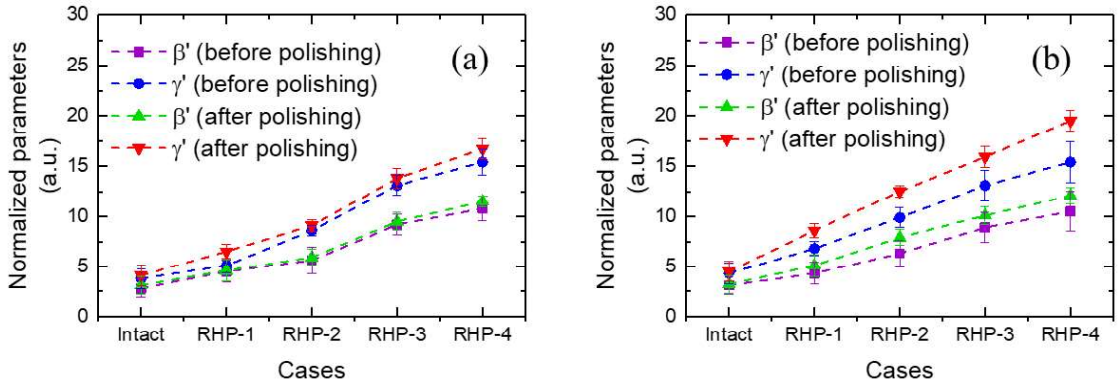

Fig. 10. Comparison of the nonlinearity parameters recorded before and after polishing the peened specimens. (a) LCR waves and (b) Rayleigh waves.

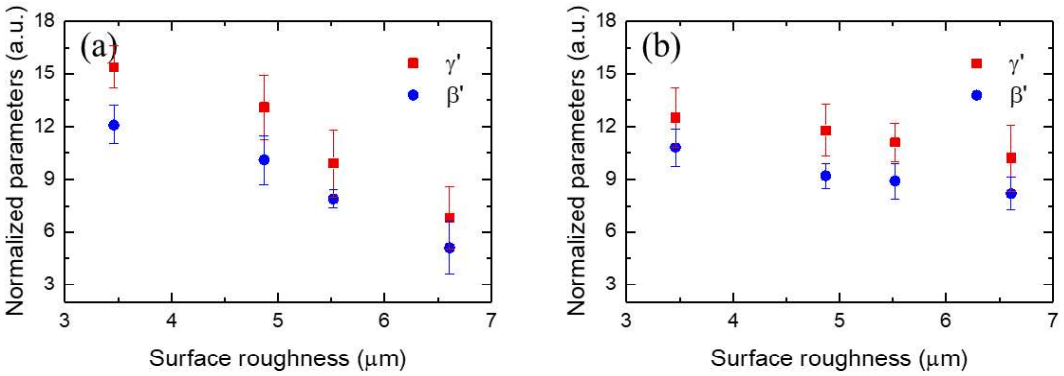

Fig. 11. Nonlinearity parameters variations for peened specimens with respect to surface roughness (R_a). (a) Rayleigh wave and (b) LCR wave.

Fig. 11 demonstrates the nonlinearity parameters of peened specimens with rough surfaces (R_a = 3.46, 4.87, 5.52, and 6.61 μm). It is observed that when Rayleigh waves traverse a surface with lower roughness, the nonlinear harmonic component measurements increase. The nonlinearity parameters of Rayleigh wave are heavily impacted by the surface roughness when compared to LCR wave. Fig. 11(a) reveals that approximately 55.8% alteration of the parameter, γ', is primarily caused by the surface roughness. In addition, the fluctuation of the parameter, γ', is greater than that of β'. This suggests that the third harmonic generation is more sensitive to the surface roughness. Therefore, the experimental results suggest that the surface roughness has a greater influence on the nonlinearity parameter measurements.

5. Conclusions

In this study, the residual stress induced by robotic hammer peening (RHP) near the surfaces of metallic structures was investigated using nonlinear ultrasonics based on the second- and third-harmonic components. Transmitting and oblique incidence ultrasonic detection probes were designed to excite the LCR and Rayleigh waves at a certain depth for the tested specimens. The stress gradient formula was presented based on the correlation between penetration depth and the ultrasonic frequencies. The residual stress profile was determined experimentally using the second

and third harmonic components of the LCR and Rayleigh waves. The results of nonlinear ultrasonic testing reveal a considerable increase in the acoustic nonlinearity parameter with an increase in peening intensities, suggesting the potential of nonlinear ultrasonics for the evaluation of near-surface residual stresses. It was found that the third harmonic component of ultrasonic waves was more sensitive to residual stress than the second harmonic component. Furthermore, the surface roughness of a specimen has a considerable impact on the nonlinear third harmonic component, similar to second harmonic component measurements. However, the current method shows difficulty in determining the location of the maximum compressive residual stress due to the low frequency ultrasonic surface waves (5 MHz) used. Future research should focus on enhancing the depth profiling resolution through the application of high frequency (> 30 MHz) LCR and Rayleigh waves.

CRediT authorship contribution statement

Santhakumar Sampath: Conceptualization, Methodology, Writing – original draft. **Hongfei Liu:** Analysis of data, Resources, Writing – review & editing. **Zi Wen Tham:** Acquisition of data. **Yi Fan Chen:** Acquisition of data. **Lei Zhang:** Conceptualization, Writing – review & editing, Supervision.

Declaration of competing interest:

The authors declare that they have no known competing financial interests or personal relationships that could have appeared to influence the work reported in this paper.

Acknowledgement

This research is supported by the Singapore National Research Foundation under its Central GAP Fund (Grant Reference NRF2020NRF-CG001-035, Project No. SC25/21-706317).

Appendix A. Analytical model of RHP-induced residual stress

As shown in Fig. 3, the generation of a plastic zone during each impact from the hammer head constrains the plastic deformation zone. When the hammer impacts, it produces residual stress throughout the structure due to the interaction between the plastic and elastic zones. This residual stress is the sum of all the fields caused by repeated impacts covering the entire structural surface. It is assumed that the hammer shot is elastic, and the target is a semi-infinite elastic solid, which is similarly assumed in the analytical model of the shot peening approach [68]. The equation of motion during contact of the hammer head with an elastic solid is defined as [68]:

$$\frac{4}{3}\pi\rho R^3\frac{dV}{dT} = -\pi a^2 p \tag{A1}$$

where ρ denotes the material density, R denotes the radius of the hammer head, V is the speed of the hammer head, T represents the time, and a is the contact radius of the hammer head. p is the average contact pressure, defined as [69]:

$$p = \sigma_Y\left(0.6 + \frac{2}{3}\ln\frac{Ea}{\sigma_Y R}\right) \tag{A2}$$

where σ_Y is the yield stress and E is the Young's modulus. Substituting Eq. (A2) into Eq. (A1), the velocity of the hammer head can be obtained by assuming that p remains constant during peening, yielding Eq. (A3) [70]:

$$V = \left(\frac{d}{R}\right)^2\left(\frac{3p}{2\rho}\right) \tag{A3}$$

where d is the indentation depth. The depth of the plastic deformation zone, h_p, is expressed as follows [71]:

$$h_p = 3R\left(\frac{d}{R}\right)^{1/2} \tag{A4}$$

In addition, the radial diameter of the plastic deformation zone ϕ, shown in Fig. A1, can be expressed as follows [72]:

$$\phi = \delta h_p \tag{A5}$$

where δ is an experimentally determined coefficient.

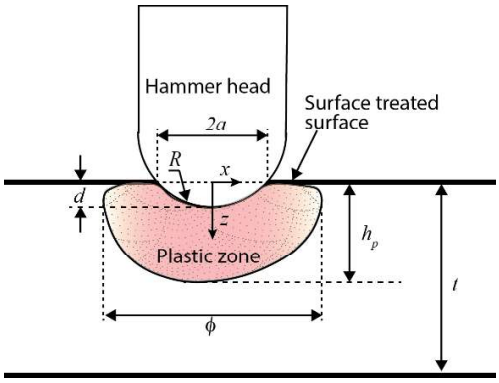

Fig. A1. Schematic illustration of the plastic deformation induced by hammer peening.

Furthermore, the residual stress, $\sigma_R(z)$, induced by hammer peening in an isotropic solid, can be expressed as [73]:

$$\sigma_R(z) = \frac{E}{1-\nu}\left[\frac{12\lambda}{\pi h_p}(1-\alpha)\left(\frac{t}{2}-z\right)P_1 + \frac{2\lambda}{\pi}(1-\alpha)P_2 - \frac{\epsilon(z)}{\epsilon_m}\right] \tag{A6}$$

where

$$\lambda = \frac{h_p}{t},$$

$$P_1 = P_2 - 2\lambda + \frac{4\lambda}{\pi}(1-\alpha)cos\frac{\pi\alpha}{2(1-\alpha)},$$

$$P_2 = 1 + sin\frac{\pi\alpha}{2(1-\alpha)}, \tag{A7}$$

$$\alpha = \frac{R}{h_p + R}$$

where λ and α are the coefficients to be determined experimentally, t is the specimen thickness, ν denotes the poisson's ratio. z is the coordinate along the thickness direction. As a result of the interactions between the plastic zones and elastic field, the residual compressive stress becomes localized in the plastic zones. The simplified form of Eq. (A7) can be used to describe the residual stress profile within the plastic deformation zone [73]:

$$\sigma_R(z) \approx E\left[-1 + 2\ln\left(\frac{z+R}{h_p+R}\right)\right] \text{ when } 0 \le z \le h_p$$
$$\sigma_R(z) \approx 0 \text{ when } h_p \le z \le t \tag{A8}$$

Using the value of h_p obtained from Eq. (A4), the residual stress distribution can be directly obtained from the RHP parameters.

References

[1] P. Withers, Residual stress and its role in failure, Reports on progress in physics, 70 (2007) 2211.
[2] E. Maleki, O. Unal, M. Guagliano, S. Bagherifard, The effects of shot peening, laser shock peening and ultrasonic nanocrystal surface modification on the fatigue strength of Inconel 718, Materials Science and Engineering: A, 810 (2021) 141029.
[3] H. Liu, T.L. Meng, J. Cao, C.K.I. Tan, Advanced Surface Engineering and Protective Coating, in, Springer Singapore, Singapore, 2022, pp. 138-141.
[4] A. Azhari, S. Sulaiman, A.P. Rao, A review on the application of peening processes for surface treatment, in: IOP Conference Series: Materials Science and Engineering, IOP Publishing, 2016, pp. 012002.
[5] N. Gong, T. Luai Meng, C. Kiang Ivan Tan, J. Cao, Y. Wei, N. Maharjan, D.C.C. Tan, H. Xie, C.J.J. Lee, R.D.K. Misra, H. Liu, High energy laser-shock induced phase transformation and micro-spallation on surface of stainless steels: The effect of stacking fault energy and deformation mechanisms, Applied Surface Science, 613 (2023) 156013.
[6] H. Liu, Y. Wei, C.K.I. Tan, D.T. Ardi, D.C.C. Tan, C.J.J. Lee, XRD and EBSD studies of severe shot peening induced martensite transformation and grain refinements in austenitic stainless steel, Materials Characterization, 168 (2020) 110574.
[7] P. Bouchard, Residual stresses in lifetime and structural integrity assessment, Encyclopedia of materials: science and technology, (2001) 8134-8142.
[8] P. Siahpour, M. Amegadzie, E. Moreau, D. Kalliecharan, T. Monchesky, A. Tieu, B. Christensen, I. Donaldson, K. Plucknett, Surface characteristics and residual stress generation in Ti-6Al-4 V following ultrasonic pulsed water jet peening, Surface and Coatings Technology, 445 (2022) 128691.

[9] J. Zhao, J. Tang, W. Zhou, T. Jiang, H. Liu, B. Xing, Numerical modeling and experimental verification of residual stress distribution evolution of 12Cr2Ni4A steel generated by shot peening, Surface and Coatings Technology, 430 (2022) 127993.
[10] Q. Lin, H. Liu, C. Zhu, R.G. Parker, Investigation on the effect of shot peening coverage on the surface integrity, Applied Surface Science, 489 (2019) 66-72.
[11] H. Liu, C.K.I. Tan, W.S. Cheng, G.W. Lim, D.C. Tan, C.J. Lee, J.J. Cheng, H.K. Cheng, L.C. Lee, Effects of robotic hammer peening on structural properties of Ni-based single-crystal superalloy: dislocation slip traces and crystallographic reorientations, Metallurgical and Materials Transactions A, 51 (2020) 3180-3193.
[12] B. Nagarajan, D. Kumar, Z. Fan, S. Castagne, Effect of deep cold rolling on mechanical properties and microstructure of nickel-based superalloys, Materials Science and Engineering: A, 728 (2018) 196-207.
[13] J. Chi, Z. Cai, Z. Wan, H. Zhang, Z. Chen, L. Li, Y. Li, P. Peng, W. Guo, Effects of heat treatment combined with laser shock peening on wire and arc additive manufactured Ti17 titanium alloy: Microstructures, residual stress and mechanical properties, Surface and Coatings Technology, 396 (2020) 125908.
[14] W.L. Chan, K.H. Low, H.K.F. Cheng, R. Chan, Effect of Overlap in Robotic Hammer Peening on the Surface Integrity of Alloy Steel 4142, in: International Conference on Advanced Surface Enhancement, Springer, 2021, pp. 45-48.
[15] W.L. Chan, H.K.F. Cheng, Hammer peening technology—the past, present, and future, The International Journal of Advanced Manufacturing Technology, (2021) 1-19.
[16] N. Gong, T.L. Meng, J. Cao, Y. Wang, R. Karyappa, C.K. Ivan Tan, A. Suwardi, Q. Zhu, A.C.Y. Ngo, K.P. Misra, R.D.K. Misra, H. Liu, Laser-cladding of high entropy alloy coatings: an overview, Materials Technology, 38 (2023) 2151696.
[17] W.Y.S. Lim, J. Cao, A. Suwardi, T.L. Meng, C.K.I. Tan, H. Liu, Recent advances in laser-cladding of metal alloys for protective coating and additive manufacturing, Journal of Adhesion Science and Technology, 36 (2022) 2482-2504.
[18] H. Liu, C.K.I. Tan, X. Dong, T.L. Meng, J. Cao, Y. Wei, Laser-cladding and robotic hammer peening of stainless steel 431 on low alloy steel 4140 for surface enhancement and corrosion protections, Journal of Adhesion Science and Technology, 36 (2022) 2313-2327.
[19] G. Jiang, F. Haiyang, P. Bo, K. Renke, Recent progress of residual stress measurement methods: A review, Chinese Journal of Aeronautics, 34 (2021) 54-78.
[20] P. Withers, M. Turski, L. Edwards, P. Bouchard, D. Buttle, Recent advances in residual stress measurement, International Journal of Pressure Vessels and Piping, 85 (2008) 118-127.
[21] J. Lin, N. Ma, Y. Lei, H. Murakawa, Measurement of residual stress in arc welded lap joints by cosα X-ray diffraction method, Journal of Materials Processing Technology, 243 (2017) 387-394.
[22] P.S. Prevey, X-ray diffraction residual stress techniques, ASM International, ASM Handbook., 10 (1986) 380-392.
[23] R. Coppola, F. Crescenzi, W. Gan, M. Hofmann, M. Li, E. Visca, J.-H. You, Neutron diffraction measurement of residual stresses in an ITER-like tungsten-monoblock type plasma-facing component, Fusion Engineering and Design, 146 (2019) 701-704.
[24] F. Foadian, A. Carradó, T. Pirling, H. Palkowski, Residual stresses evolution in Cu tubes, cold drawn with tilted dies–Neutron diffraction measurements and finite element simulation, Materials & Design, 107 (2016) 163-170.

[25] M.R. Daymond, N.W. Bonner, Measurement of strain in a titanium linear friction weld by neutron diffraction, Physica B: Condensed Matter, 325 (2003) 130-137.
[26] M. Masoomi, N. Shamsaei, R.A. Winholtz, J.L. Milner, T. Gnäupel-Herold, A. Elwany, M. Mahmoudi, S.M. Thompson, Residual stress measurements via neutron diffraction of additive manufactured stainless steel 17-4 PH, Data in brief, 13 (2017) 408-414.
[27] D. Brown, J. Bernardin, J. Carpenter, B. Clausen, D. Spernjak, J. Thompson, Neutron diffraction measurements of residual stress in additively manufactured stainless steel, Materials Science and Engineering: A, 678 (2016) 291-298.
[28] D.W. Brown, M.A. Okuniewski, T.A. Sisneros, B. Clausen, G.A. Moore, L. Balogh, Neutron diffraction measurement of residual stresses, dislocation density and texture in Zr-bonded U-10Mo "mini" fuel foils and plates, Journal of Nuclear Materials, 482 (2016) 63-74.
[29] R. Acevedo, P. Sedlak, R. Kolman, M. Fredel, Residual stress analysis of additive manufacturing of metallic parts using ultrasonic waves: State of the art review, Journal of Materials Research and Technology, 9 (2020) 9457-9477.
[30] A. Vasu, R.V. Grandhi, Impact of plasticity generated by Rayleigh waves on the residual stress behavior of structural components subjected to laser peening, International Journal of Structural Integrity, 6 (2015) 107-123.
[31] Y. Javadi, G.M. Krolczyk, S. Hloch, Evaluation of hoop residual stress variations in the thickness of dissimilar welded pipes by using the LCR ultrasonic waves, Tehnicki Vjesnik, 23 (2016) 329-335.
[32] P. Mora, M. Spies, Rayleigh wave harmonic generation in materials with depth-dependent non-linear properties, The Journal of the Acoustical Society of America, 143 (2018) 2678-2684.
[33] F. Belahcene, J. Lu, Determination of residual stress in Z8CDWV12 steel using critically refracted longitudinal waves, JSME International Journal Series A Solid Mechanics and Material Engineering, 43 (2000) 367-373.
[34] Y. Pan, M. Qian, W.-J. Xu, M. Ourak, Residual stress profiling of an aluminum alloy by laser ultrasonics, (2004).
[35] M. Hirao, H. Fukuoka, K. Hori, Acoustoelastic effect of Rayleigh surface wave in isotropic material, (1981).
[36] A. Zeiger, K. Jassby, Measurement of acoustoelastic coefficients of Rayleigh waves in steel alloys, Journal of Nondestructive Evaluation, 3 (1982) 115-124.
[37] E. Hu, Y. He, Y. Chen, Experimental study on the surface stress measurement with Rayleigh wave detection technique, Applied Acoustics, 70 (2009) 356-360.
[38] M. Rjelka, M. Barth, S. Reinert, B. Koehler, J. Bamberg, H.U. Baron, R. Hessert, Third order elastic constants and rayleigh wave dispersion of shot peened aero-engine materials, in: Materials Science Forum, Trans Tech Publ, 2014, pp. 201-208.
[39] Y. Zhan, H. Xu, W. Du, C. Liu, Research on the influence of heat treatment on residual stress of TC4 alloy produced by laser additive manufacturing based on laser ultrasonic technique, Ultrasonics, 115 (2021) 106466.
[40] Z. Liu, B. Lin, X. Liang, A. Du, Inversion of surface damage and residual stress in ground silicon wafers by laser surface acoustic wave technology, Ultrasonics, 113 (2021) 106367.
[41] Z. Yang, H. Yang, T. Tian, D. Deng, M. Hu, J. Ma, D. Gao, J. Zhang, S. Ma, L. Yang, A review in guided-ultrasonic-wave-based structural health monitoring: From fundamental theory to machine learning techniques, Ultrasonics, (2023) 107014.
[42] J. Yue, X. Hong, B. Zhang, An intelligent colony optimization imaging method for composites health monitoring using ultrasonic guided wave, Ultrasonics, 132 (2023) 107019.

[43] S. Zhang, X. Li, H. Jeong, H. Hu, Experimental investigation of material nonlinearity using the Rayleigh surface waves excited and detected by angle beam wedge transducers, Ultrasonics, 89 (2018) 118-125.
[44] S. Basu, A. Thirumalaiselvi, S. Sasmal, T. Kundu, Nonlinear ultrasonics-based technique for monitoring damage progression in reinforced concrete structures, Ultrasonics, 115 (2021) 106472.
[45] S. Sampath, H. Sohn, Cubic nonlinearity parameter measurement and material degradation detection using nonlinear ultrasonic three-wave mixing, Ultrasonics, 121 (2022) 106670.
[46] S. Park, T. Kundu, A modified sideband peak count based nonlinear ultrasonic technique for material characterization, Ultrasonics, 128 (2023) 106858.
[47] A. Bellotti, J.-Y. Kim, J.E. Bishop, B.H. Jared, K. Johnson, D. Susan, P.J. Noell, L.J. Jacobs, Nonlinear ultrasonic technique for the characterization of microstructure in additive materials, The Journal of the Acoustical Society of America, 149 (2021) 158-166.
[48] G. Shui, Y.-S. Wang, F. Gong, Evaluation of plastic damage for metallic materials under tensile load using nonlinear longitudinal waves, NDT & E International, 55 (2013) 1-8.
[49] J.S. Valluri, K. Balasubramaniam, R.V. Prakash, Creep damage characterization using non-linear ultrasonic techniques, Acta Materialia, 58 (2010) 2079-2090.
[50] S. Quan, Y. Zhang, Y. Li, P. Lin, Near surface residual stress detection of metallic materials using the high order ultrasonic nonlinear coefficient, Materials Express, 13 (2023) 688-694.
[51] Y.-H. Zhang, X.-X. Li, X.-H. Wang, Z.-F. Huang, H.-L. Mao, H.-Y. Mao, Feasibility of residual stress nondestructive estimation using the nonlinear property of critical refraction longitudinal wave, Advances in Materials Science and Engineering, 2017 (2017).
[52] F. Belahcene, J. Lu, Determination of residual stress using critically refracted longitudinal waves and immersion mode, The Journal of Strain Analysis for Engineering Design, 37 (2002) 13-20.
[53] W. Song, C. Xu, Q. Pan, J. Song, Nondestructive testing and characterization of residual stress field using an ultrasonic method, Chinese Journal of Mechanical Engineering, 29 (2016) 365-371.
[54] S. Sadeghi, M.A. Najafabadi, Y. Javadi, M. Mohammadisefat, Using ultrasonic waves and finite element method to evaluate through-thickness residual stresses distribution in the friction stir welding of aluminum plates, Materials & Design (1980-2015), 52 (2013) 870-880.
[55] H. Mao, Q. Li, H. Mao, Z. Huang, W. Tang, H. Huang, X. Yi, G. Qing, X. Li, Nonlinear ultrasonic characterization of carburized case depth, NDT & E International, 112 (2020) 102244.
[56] M. Liu, J.-Y. Kim, L. Jacobs, J. Qu, Experimental study of nonlinear Rayleigh wave propagation in shot-peened aluminum plates—Feasibility of measuring residual stress, Ndt & E International, 44 (2011) 67-74.
[57] J.H. Cantrell, Substructural organization, dislocation plasticity and harmonic generation in cyclically stressed wavy slip metals, Proceedings of the Royal Society of London. Series A: Mathematical, Physical and Engineering Sciences, 460 (2004) 757-780.
[58] J.-Y. Kim, J. Qu, L. Jacobs, J. Littles, M. Savage, Acoustic nonlinearity parameter due to microplasticity, Journal of Nondestructive Evaluation, 25 (2006) 28-36.
[59] S.-J. Bang, D.-G. Song, K.-Y. Jhang, Comparisons of second-and third-order ultrasonic nonlinearity parameters measured using through-transmission and pulse-echo methods, NDT & E International, 133 (2023) 102757.
[60] H. Hu, Z. Zou, Y. Jiang, X. Wang, K. Yi, Finite element simulation and experimental study of residual stress testing using nonlinear ultrasonic surface wave technique, Applied Acoustics, 154 (2019) 11-17.

[61] G. Ren, J. Kim, K.-Y. Jhang, Relationship between second-and third-order acoustic nonlinear parameters in relative measurement, Ultrasonics, 56 (2015) 539-544.
[62] S. Gebrekidan, T. Kang, H.-J. Kim, S.-J. Song, Nonlinear ultrasonic characterization of early degradation of fatigued Al6061-T6 with harmonic generation technique, Ultrasonics, 85 (2018) 23-30.
[63] J.K. Na, M.A. Breazeale, Ultrasonic nonlinear properties of lead zirconate- titanate ceramics, The Journal of the Acoustical Society of America, 95 (1994) 3213-3221.
[64] X. Liu, B. Lin, X. Liang, Study of laser-induced surface acoustic wave propagating on materials with machined surfaces based on wavelet analysis, Surface and Coatings Technology, 358 (2019) 173-181.
[65] S. Sampath, H. Sohn, Non-contact microcrack detection via nonlinear Lamb wave mixing and laser line arrays, International Journal of Mechanical Sciences, 237 (2023) 107769.
[66] N.P. Yelve, P.W. Tse, F. Masurkar, Theoretical and experimental evaluation of material nonlinearity in metal plates using Lamb waves, Structural Control and Health Monitoring, 25 (2018) e2164.
[67] H. Liu, C.K.I. Tan, Y. Wei, G.W. Lim, W.S. Cheng, N. Maharjan, Robotic hammer peening-induced martensite in austenitic steels: spatial distributions of plastic deformation and phase transformation, Procedia CIRP, 87 (2020) 297-301.
[68] A.S. Franchim, V.S. de Campos, D.N. Travessa, C. de Moura Neto, Analytical modelling for residual stresses produced by shot peening, Materials & Design, 30 (2009) 1556-1560.
[69] K. Johnson, K. Johnson, Cambridge University Press; Cambridge, UK: 1985, Contact Mechanics.[Google Scholar].
[70] S. Al-Hassani, An engineering approach to shot peening mechanics, in: Proc. Of the second Int. Conf. On Shot Peening, 1984.
[71] X. Zhang, T. Wang, J. Wang, C. Liu, Analytical modeling of shot peen forming process using cross-sectional linear indentation coverage method, International Journal of Mechanical Sciences, 133 (2017) 838-845.
[72] H. Miao, S. Larose, C. Perron, M. Lévesque, An analytical approach to relate shot peening parameters to Almen intensity, Surface and Coatings Technology, 205 (2010) 2055-2066.
[73] Y. Al-Obaid, Shot peening mechanics: experimental and theoretical analysis, Mechanics of Materials, 19 (1995) 251-260.